

AnoleVLA: Lightweight Vision-Language-Action Model with Deep State Space Models for Mobile Manipulation

Yusuke Takagi, Motonari Kambara, Daichi Yashima, Koki Seno, Kento Tokura and Komei Sugiura

Abstract—In this study, we address the problem of language-guided robotic manipulation, where a robot is required to manipulate a wide range of objects based on visual observations and natural language instructions. This task is essential for service robots that operate in human environments, and requires safety, efficiency, and task-level generality. Although Vision-Language-Action models (VLAs) have demonstrated strong performance for this task, their deployment in resource-constrained environments remains challenging because of the computational cost of standard transformer backbones. To overcome this limitation, we propose *AnoleVLA*, a lightweight VLA that uses a deep state space model to process multimodal sequences efficiently. The model leverages its lightweight and fast sequential state modeling to process visual and textual inputs, which allows the robot to generate trajectories efficiently. We evaluated the proposed method in both simulation and physical experiments. Notably, in real-world evaluations, *AnoleVLA* outperformed a representative large-scale VLA by 21 points for the task success rate while achieving an inference speed approximately three times faster. Our code and videos are available at this URL¹.

I. INTRODUCTION

Object manipulation is essential for service robots that operate in everyday environments, and requires safety, efficiency, and task-level generality. In such environments, robots are often instructed by users through natural language, which makes language-conditioned manipulation a practical necessity. Based on this background, Vision-Language-Action models (VLAs) have been studied extensively. Despite significant advances in VLAs [1]–[3], deploying them on physical robots remains challenging because their backbones require substantial memory and compute at inference time.

Given the above background, in this study, we address language-guided robotic manipulation. A typical use case involves a robot performing pick-and-place tasks in a cluttered table-top environment. For instance, as shown in Fig. 1, given the instruction “Place the apple in the red bowl,” the robot grounds the referring expressions in the instruction to the specific objects in the scene to identify the target apple among various distractors and moves it to the designated container.

Although VLAs [1]–[6] demonstrate strong performance in such manipulation tasks, deploying them under resource constraints remains challenging, because their backbone constitutes a major source of inference latency and memory consumption. For example, OpenVLA builds on Llama-2

The authors are with Keio University, 3-14-1 Hiyoshi, Kohoku, Yokohama, Kanagawa 223-8522, Japan. yusuke.10.06@keio.jp

This work was partially supported by JSPS KAKENHI Grant Number 23K28168, JST Moonshot, and JSPS Fellows Grant Number JP23KJ1917.

¹<https://anolevla-8z7l8.kinsta.page/>

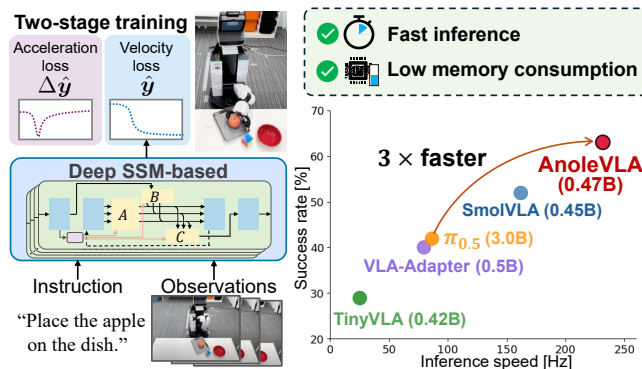


Fig. 1: Overview of AnoleVLA and real-world performance. (Left) Our deep SSM backbone processes language instructions and robot observations to generate trajectories, leveraging a two-stage training strategy with the acceleration loss for smooth control. (Right) Physical experiment results. The horizontal and vertical axes represent inference speed and the average success rate, respectively. AnoleVLA achieved the highest overall success rate. Notably, compared with $\pi_{0.5}$, AnoleVLA not only yielded superior task performance but also demonstrated an inference speed approximately three times faster.

7B [3], and even the comparatively compact $\pi_{0.5}$ uses a 3B-parameter language model [1]. A key bottleneck is backbone sequence modeling based on transformers. Transformer self-attention scales quadratically with sequence length, which becomes problematic because VLAs typically concatenate vision, language, and robot-state tokens into a single sequence. As the number of vision tokens or temporal context grows, this quadratic cost can be a critical bottleneck for real-time deployment on resource-constrained platforms.

To overcome this limitation, we propose *AnoleVLA*, a lightweight VLA that leverages a deep state space model (deep SSM) for efficient multimodal sequence modeling. By leveraging the linear computational complexity of deep SSMs, this model addresses the inference bottlenecks.

The main differences between AnoleVLA and prior VLAs are the adoption of a state space backbone to circumvent the quadratic scaling of transformer layers and its ability to directly generate continuous action trajectories without discretization. Unlike typical VLAs, AnoleVLA uses a deep SSM, which maintains a recurrent state and updates it with linear complexity, enabling long-context multimodal conditioning under limited computation and memory budgets. Additionally, unlike many existing VLAs [3], [4], [7] that discretize continuous actions into tokens to use the language model’s autoregressive decoding, AnoleVLA directly generates continuous actions from the final hidden state of the backbone.

The main contributions of this study are summarized as follows:

- We propose a lightweight VLA for resource-constrained deployment, which reduces inference latency and VRAM usage for long-context multimodal inputs.
- We introduce a deep SSM backbone architecture and leverage its computationally efficient sequence processing capabilities for VLA modeling.
- We introduce a two-stage training strategy that uses the acceleration loss in the second phase to refine the policy learned through the velocity loss.

II. RELATED WORK

A. Vision-Language-Action Models

Pre-trained vision-language models have been adopted increasingly in robotics [1], [8]–[10]. As surveyed in [11], [12], VLAs have emerged as one of the most prominent approaches for language-conditioned manipulation [1], [5], [13]–[15], where a pre-trained vision-language model is fine-tuned on robot demonstration data [1], [3], [4], [7]. However, these models are built on multimodal large language models (MLLMs), often exceeding 7 billion parameters [3], [4], and are slow during inference, which makes real-world deployment difficult [14], [15]. To address these issues, several works have investigated smaller-scale VLAs that reduce inference cost [13]–[15].

In addition to architectural design, the choice of training data is a key factor in VLA performance. Open X-Embodiment (OXE) [16] aggregates trajectory data from multiple robot platforms, including Fractal [17] and Bridge-Data V2 [18], and includes a lot of manipulation episodes paired with language instructions. OXE has become a standard training source for many VLAs [3], [16], [19]–[21]. For evaluation, simulation benchmarks are widely used because they offer reproducibility at lower cost. Meta-World [22] defines diverse manipulation tasks on a single robot arm and has been adopted in several studies [14], [15].

B. Deep State Space Models

Deep SSMs model sequences via a recurrent state that is updated at each timestep, which offers linear complexity in sequence length as an alternative to the quadratic cost of transformer self-attention [23], [24]. S4 introduced structured parameterizations to handle long-range dependencies [23] and Mamba further introduced input-dependent selection mechanisms that control information propagation over the sequence [25]. These backbones have been adopted in multimodal language models such as Cobra, VL-Mamba, and EMMA, with an emphasis on efficient long-context processing [26]–[28].

In robotics, deep SSMs have been adopted in various ways depending on where state space recurrence is placed in the learning and control pipeline. Some VLAs use deep SSM backbones to map multimodal tokens to end-effector representation. For example, RoboMamba predicts contact points and end effector pose with a lightweight head [29]. Deep SSMs have also been used as multimodal fusion modules. FlowRAM integrates Mamba blocks within a conditional flow matching pipeline [30]. Other studies (e.g. [31], [32])



Fig. 2: Typical scene of the language-guided manipulation task. The frames illustrate the robot’s execution in chronological order from left to right. In this scene, the robot is given the instruction, “Place the apple into the red bowl.” The robot successfully grasps the apple from among multiple fruits and places it in the bowl.

used state space recurrence for world models or for long-horizon imitation learning.

Another research direction involves the study of deep SSM backbones for visuo-motor policy learning, where policies map sensory inputs to end-effector trajectory representation under imitation learning or generative objectives. This includes Mamba-based diffusion policies and proprioceptive motion encoders [33]–[36].

Compared with these visuo-motor and generative policy formulations, AnoleVLA differs in two key aspects. First, we train for execution smoothness by supervising both the end-effector trajectory and temporal differences with a two-stage training strategy. Second, AnoleVLA generates a short-horizon continuous action chunk from multimodal tokens in a single forward pass, without action discretization or iterative inference. As a result, AnoleVLA targets language-guided manipulation settings where smooth continuous trajectories and efficient inference are both important.

III. PROBLEM STATEMENT

In this study, we address the task of language-guided robotic manipulation. In this task, the robot is required to appropriately manipulate objects as specified by the language instructions.

Fig. 2 shows an example of the task. The sequence of images presents the robot’s execution in chronological order. In this example, given the instruction “Place the apple in the red bowl,” the robot arm successfully grasps the apple and places it into the red bowl, following the instruction.

The input to the task consists of images, proprioceptive state, and a natural language instruction. The output is the robot’s trajectory, formulated as a sequence of actions $\hat{\mathbf{y}}^{(1:H)} \in \mathbb{R}^{d_a \times H}$, where d_a and H denote the dimension of the action space and the action chunking length, respectively. We use the success rate and inference speed as the evaluation metrics.

IV. PROPOSED METHOD

AnoleVLA is closely related to Mamba [25]-based MLLMs, including Cobra [26], VL-Mamba [27], and EMMA [28]. The architectural frameworks of these models can be adapted to many existing VLAs [1], [5], [13]. Because both Mamba and transformers operate as causal sequence models over a shared token space, Mamba can seamlessly replace the transformer backbone while preserving the upstream multimodal tokenization and downstream

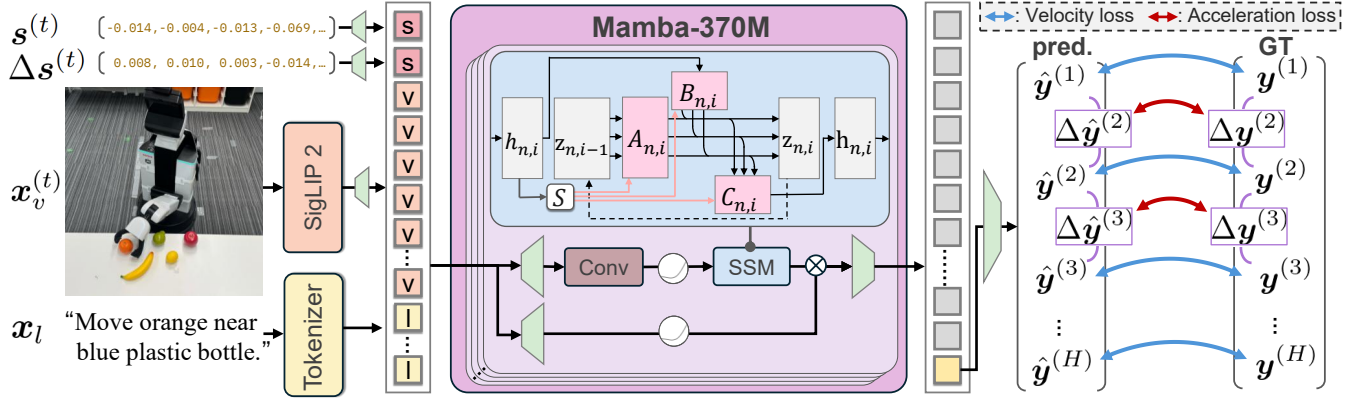


Fig. 3: Model architecture of AnoleVLA. Multimodal tokens (proprioception, state delta, vision, and language) are concatenated and processed by a Mamba backbone, and the final token predicts an H -step action chunk. The two-stage training supervises both velocities and their temporal differences to improve execution smoothness. In this figure, $\mathbf{s}^{(t)}$, $\Delta \mathbf{s}^{(t)}$, $\mathbf{x}_v^{(t)}$, and \mathbf{x}_l represent the state, state delta, visual observation, and natural language instruction at time step t , respectively. On the right-hand side, ‘pred.’ and ‘GT’ denote the predicted outputs and the corresponding ground truth, respectively. Specifically, $\hat{\mathbf{y}}$ and \mathbf{y} represent the predicted future actions and their ground truth, respectively. Furthermore, $\Delta \hat{\mathbf{y}}$ and $\Delta \mathbf{y}$ denote the temporal differences of $\hat{\mathbf{y}}$ and \mathbf{y} , respectively.

action decoding pipelines. The main novelty of this work can be summarized as follows:

- We propose a lightweight and high-speed VLA designed to operate efficiently, even in resource-constrained environments.
- We use Mamba as the backbone architecture and leverage its computationally efficient sequence processing capabilities for VLA modeling.
- We introduce a two-stage training strategy that uses the acceleration loss in the second phase, which complements the velocity loss used in the initial phase.

A. Preliminaries: Mamba

Deep SSMs have become effective substitutes for transformers because of their linear scalability with sequence length L . In particular, transformer self-attention scales quadratically as $\mathcal{O}(L^2)$, whereas deep SSM-based models process sequences in $\mathcal{O}(L)$ time, which enables efficient long-context modeling.

Mamba [25] is a selective deep SSM that introduces an input-dependent selection mechanism, which allows the model to dynamically propagate or forget information along the token sequence. We adopt Mamba as the backbone in AnoleVLA’s architecture while keeping the same multimodal tokenization and action decoding pipeline.

B. Architecture

Fig. 3 illustrates the overall architecture of AnoleVLA, which consists of three components: an input embedding module, Mamba backbone, and action head.

a) Input embedding module: We define the model input at time step t , denoted by $\mathbf{x}^{(t)}$, as follows:

$$\mathbf{x}^{(t)} = \{\mathbf{s}^{(t)}, \Delta \mathbf{s}^{(t)}, \mathbf{x}_v^{(t)}, \mathbf{x}_l\}, \quad (1)$$

where $\mathbf{s}^{(t)}$, $\Delta \mathbf{s}^{(t)} (:= \mathbf{s}^{(t)} - \mathbf{s}^{(t-1)})$, $\mathbf{x}_v^{(t)}$, and \mathbf{x}_l represent the robot state, delta state, RGB images, and natural language instruction, respectively. The input embedding module projects each component of $\mathbf{x}^{(t)}$ into a shared latent space of dimension D . Specifically, $\mathbf{s}^{(t)}$ and $\Delta \mathbf{s}^{(t)}$ are each mapped

via linear projections to single-token embeddings $\mathbf{h}_s^{(t)} \in \mathbb{R}^D$ and $\mathbf{h}_{\Delta s}^{(t)} \in \mathbb{R}^D$, respectively. $\mathbf{x}_v^{(t)}$ is encoded using SigLIP 2 [37], initialized with pre-trained weights, and fine-tuned end-to-end on robot demonstration data, followed by a linear projection, which yields visual tokens $\mathbf{h}_v^{(t)} \in \mathbb{R}^{N_v \times D}$, where N_v denotes the visual tokens’ sequence length. Then \mathbf{x}_l is tokenized and projected by a linear layer to obtain $\mathbf{h}_l \in \mathbb{R}^{N_l \times D}$, where N_l denotes the sequence length. These embeddings are concatenated to form the input sequence:

$$\mathbf{H}_0 = [\mathbf{h}_s^{(t)}, \mathbf{h}_{\Delta s}^{(t)}, \mathbf{h}_v^{(t)}, \mathbf{h}_l] \in \mathbb{R}^{L \times D}, \quad (2)$$

where $L = 2 + N_v + N_l$ is the total number of tokens, with the constant 2 accounting for $\mathbf{h}_s^{(t)}$ and $\mathbf{h}_{\Delta s}^{(t)}$. We place proprioceptive tokens at the beginning of the sequence so that, under Mamba’s causal recurrence, the hidden state is first conditioned on the agent’s state before the integration of visual and linguistic information.

b) Mamba backbone: The backbone consists of K stacked Mamba blocks. Each block comprises a selective deep SSM layer, a SiLU-gated linear unit, layer normalization, and a residual connection, following [25]. For notational convenience, we index the input sequence positionally as $\mathbf{H}_0 = [\mathbf{h}_{0,1}, \dots, \mathbf{h}_{0,L}]$. The n -th block takes the output of the preceding block, $\mathbf{H}_{n-1} = [\mathbf{h}_{n-1,1}, \dots, \mathbf{h}_{n-1,L}]$, and applies the deep selective SSM update for each token position i :

$$\begin{aligned} \mathbf{z}_{n,i} &= \mathbf{A}_{n,i} \mathbf{z}_{n,i-1} + \mathbf{B}_{n,i} \mathbf{h}_{n-1,i}, \\ \tilde{\mathbf{h}}_{n,i} &= \mathbf{C}_{n,i} \mathbf{z}_{n,i}, \end{aligned} \quad (3)$$

where $\mathbf{z}_{n,i}$ denotes the latent state at the n -th block and the i -th token position. Moreover, $\mathbf{A}_{n,i}$, $\mathbf{B}_{n,i}$, and $\mathbf{C}_{n,i}$ are system matrices. The intermediate output $\tilde{\mathbf{h}}_{n,i}$ is then passed through the SiLU-gated linear unit, layer normalization, and a residual connection to obtain the block output $\mathbf{h}_{n,i}$.

The recurrent state update can be interpreted as a filtering process that continuously refines a running estimate of task-relevant information as new tokens arrive, aligning naturally with robotic manipulation where the model is required to incrementally integrate visual observations to determine

TABLE I: Experimental settings of AnoleVLA.

Batch Size	16
Optimizer	AdamW ($\beta_1 = 0.9, \beta_2 = 0.999$)
Learning Rate	1.0×10^{-5}
Weight Decay	1.0×10^{-2}
#Steps	400k (1st stage: 200k, 2nd stage: 200k)
Action Chunk Length	50

actions. Because Mamba processes the sequence causally, token i can only aggregate information from the prefix $\{\mathbf{h}_{n-1,j}\}_{j \leq i}$ through the recurrent hidden state. This causal structure means that the interaction between modalities is governed by the token ordering defined above.

c) *Action head*: We obtain the predicted action trajectory from the final token embedding of the last block:

$$\hat{\mathbf{y}}^{(1:H)} = f_{\text{head}}(\mathbf{h}_{K,L}), \quad (4)$$

where $f_{\text{head}}(\cdot)$ denotes a linear projection. We adopt a linear projection as the action head because the Mamba backbone already extracts a sufficiently expressive representation at the final token position through its recurrent aggregation of the full input sequence.

C. Loss Function

Following standard practices [3], [38], each action $\mathbf{y}^{(\tau)}$ is modeled as the delta end-effector pose (i.e., the end-effector velocity) at horizon step τ . Therefore, the temporal difference between consecutive actions, $\Delta \mathbf{y}^{(\tau)} := \mathbf{y}^{(\tau)} - \mathbf{y}^{(\tau-1)}$, can be interpreted as end-effector acceleration. In trajectory generation, consistency in both velocity and acceleration is important for smooth execution on real hardware. Motivated by this observation, we design a two-stage loss that supervises both quantities.

In the first stage, we minimize an L1 loss on the predicted velocity (i.e., action) sequence:

$$\mathcal{L}_{\text{vel}} = \frac{1}{H} \sum_{\tau=1}^H \left\| \mathbf{y}^{(\tau)} - \hat{\mathbf{y}}^{(\tau)} \right\|_1. \quad (5)$$

In the second stage, we update the objective with an acceleration loss that supervises the temporal differences of the action sequence:

$$\mathcal{L}_{\text{acc}} = \frac{1}{H-1} \sum_{\tau=2}^H \left\| \Delta \mathbf{y}^{(\tau)} - \Delta \hat{\mathbf{y}}^{(\tau)} \right\|_1, \quad (6)$$

where $\Delta \hat{\mathbf{y}}^{(\tau)}$ is the temporal difference of $\hat{\mathbf{y}}^{(\tau)}$. The overall training objective in the second stage is $\mathcal{L}_{\text{vel}} + \lambda_{\text{acc}} \mathcal{L}_{\text{acc}}$, where λ_{acc} is the weight. This staged training allows the model to first learn an appropriate reconstruction of the reference trajectory before the acceleration term refines its temporal consistency.

V. EXPERIMENTS

A. Settings

As a simulation benchmark, we used Meta-World [22], which is widely recognized as a standard suite for language-guided robotic manipulation. The benchmark comprises a diverse suite of manipulation tasks, including object relocation and door/drawer opening, performed by a simulated Sawyer

robot arm in a table-top setting. Each sample includes egocentric RGB images, robot state, a natural language instruction, and the reference trajectory. On this benchmark, $d_a = 4$, which corresponds to the three-dimensional end-effector position and one-dimensional continuous gripper control.

Meta-World consists of 50 diverse object manipulation tasks. The Meta-World dataset comprises a total of 2,500 episodes, total word count of 320, average sentence length of 6.53 words, and average sequence length of 81.9 frames, recorded at a sampling rate of 80 Hz.

We split the 2,500 episodes into 2,000 and 500 for the training and validation sets, respectively. We used the training set to train the model and the validation set to tune the hyperparameters. We evaluated the models using the predefined evaluation episodes from the Meta-World benchmark.

Table I shows the experimental settings of AnoleVLA. AnoleVLA has approximately 467M parameters and requires 91 GFLOPs of computation. We performed training using a computer with an NVIDIA GeForce RTX 4090 GPU (24GB) and Intel Core i9-14900F processor. The training and inference times were approximately 20 hours and 216 ms/chunk, respectively. We computed the trajectory error on the validation set every 1,000 steps. We used an early stopping strategy that terminated training if the loss did not improve for N_{val} consecutive evaluations on the validation set. For final model selection, we used the model that achieved the minimum loss on the validation set. In our experiments, we set N_{val} to 10.

B. Quantitative Results

Table II shows the quantitative comparison results between AnoleVLA and the baseline methods on the Meta-World benchmark. In the table, the best score in each column is highlighted in bold, and the second-best score is underlined. We adopted SmolVLA [15], VLA-Adapter [13], and TinyVLA [14] as the baseline methods. Each uses a transformer-based language model as its backbone at a parameter scale comparable with AnoleVLA. This setup enables a controlled comparison that isolates the empirical advantages of adopting Mamba for sequence modeling over standard transformer layers. Given that $\pi_{0.5}$ [1] is widely recognized as a standard large-scale VLA, we included it as a baseline method. In the table, the success rates for SmolVLA and TinyVLA are cited directly from their original publications. By contrast, the results reported for VLA-Adapter and $\pi_{0.5}$ are based on models trained on the Meta-World dataset. We used the success rate as the evaluation metric.

AnoleVLA achieved success rates of 89.29%, 45.45%, 66.67%, and 70.00% on Easy, Medium, Hard, and Very Hard task suites, respectively. Furthermore, AnoleVLA achieved an average success rate of 67.85% across all task suites. By contrast, the baseline methods $\pi_{0.5}$, VLA-Adapter, TinyVLA, and SmolVLA achieved average success rates of 43.80%, 0.94%, 31.58%, and 57.33%, respectively. Notably, AnoleVLA outperformed SmolVLA, the strongest baseline,

TABLE II: Quantitative comparison between AnoleVLA and the baseline methods on the Meta-World benchmark and physical experiments. In the table, ‘Med.’ and ‘V.Hard’ refer to the Medium and Very Hard task suites in the Meta-World benchmark, respectively. The ‘Inf. speed’ column specifies the inference speed of each method in the physical experiments. The best results are highlighted in **bold**, and the second-best results are underlined.

[%] Method	Total Params	Meta-World					Real World					Inf. speed [ms/chunk] ↓	
		Easy	Med.	Hard	V.Hard	Avg.	Move	Pick	Open	Close	Push		Avg.
$\pi_{0.5}$ [1]	3.0B	68.20	37.30	41.70	28.00	43.80	15	20	30	100	45	42	578
VLA-Adapter [13]	0.5B	3.75	0.0	0.0	0.0	0.94	35	20	0	100	45	40	101
TinyVLA [14]	0.42B	77.60	21.50	11.40	15.80	31.58	5	15	0	90	35	29	1290
SmolVLA [15]	0.45B	<u>82.50</u>	<u>41.80</u>	<u>45.00</u>	<u>60.00</u>	<u>57.33</u>	<u>30</u>	<u>25</u>	<u>55</u>	100	<u>50</u>	<u>52</u>	309
AnoleVLA	0.47B	89.29	45.45	66.67	70.00	67.85	45	40	75	100	55	63	<u>216</u>

by 10.52 points, and surpassed $\pi_{0.5}$ by 24.05 points. These results demonstrate that AnoleVLA outperformed the baseline approaches while maintaining a competitive or smaller model size.

C. Qualitative Results

Fig. 4 presents the qualitative results of AnoleVLA compared with SmolVLA, which was the strongest baseline. Fig. 4(a) and 4(b) illustrate successful episodes achieved by AnoleVLA.

In the episode shown in (a), a blue puck and a wooden shelf were present at $t = 0$, and x_l was “Pick and place a puck onto a shelf.” AnoleVLA successfully grasped the puck and placed it onto the shelf. By contrast, although the baseline method approached the vicinity of the puck, it failed to grasp it and moved toward the shelf, which resulted in failure.

In the episode depicted in Fig. 4(b), a hammer and a screw on a wooden block were present at $t = 0$, and x_l was “Hammer a screw on the wall.” AnoleVLA appropriately grasped the hammer and struck the screw. Conversely, although the baseline method grasped the hammer, it failed to complete the task because it swung the tool along an incorrect trajectory, thereby missing the screw. These results demonstrate that AnoleVLA was capable of generating complex trajectories that used a tool appropriately to interact with a target object conditioned on language instructions.

Fig. 4(c) illustrates a failure case of AnoleVLA. In this episode, initialized at $t = 0$, a red puck and green goal point were present on the table, and x_l was “Push the puck to a goal.” AnoleVLA failed because it could not make appropriate contact with the puck; it moved the arm past it instead of pushing it toward the goal. Similarly, the baseline method also failed by missing the target puck entirely. These results suggest that appropriately localizing the target object and generating precise contact trajectories for achieving tasks remain challenging.

D. Ablation Studies

To validate the effectiveness of AnoleVLA, we conducted ablation studies on the two-stage training strategy. Table III shows the ablation results on the Meta-World benchmark. The table presents the average success rates. Specifically, we omitted the second training stage to investigate its influence

TABLE III: Quantitative results of the ablation studies. The table presents the average success rates on the Meta-World benchmark. The best score for each metric is in bold.

Model	Acceleration Loss	SR [%]
(i)	-	63.12
(ii)	✓	67.85

TABLE IV: Categorization of failure cases. We selected a total of 20 samples and manually conducted a detailed error analysis.

Error	#Error
(i) Position recognition error	10
(ii) Grasp point prediction error	6
(iii) Incomplete motion execution	4
Total	20

on performance. Table III shows that model (i) achieves a success rate 4.73 points lower than model (ii). This result suggests that the introduction of the acceleration loss alongside the velocity loss enabled the generation of smoother and more stable trajectories, which effectively improved overall performance.

E. Error Analysis

We performed a failure analysis on 20 failed manipulation episodes to identify common failure modes. Table IV summarizes the failure cases across categories.

We define the categories as follows: (i) **Position recognition error** refers to cases in which the arm moves to a location that does not correspond to the object specified in the instruction. (ii) **Grasping point prediction error** refers to cases in which the gripper reaches the target object, but attempts to grasp an inappropriate point, which leads to failure. (iii) **Incomplete motion execution** refers to episodes in which the trajectory starts appropriately, but terminates before completing the manipulation.

Position recognition error was the most frequent failure mode. Manual inspection of the failed episodes suggests that the model often generated grasping motions toward incorrect regions or empty space, which indicates inappropriate localization of the target object from visual observations. This may reflect a limitation in extracting precise spatial information from the input images.

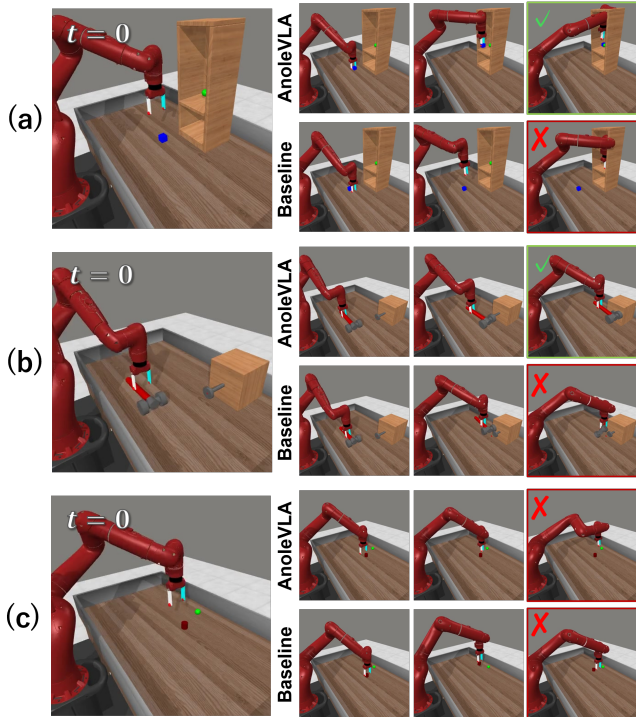


Fig. 4: Qualitative results of AnoleVLA and a baseline method. For each example, we display the initial observation $x_v^{(0)}$ and the chronological sequence of observations $x_v^{(t)}$ during task execution. In each example, the robot executes the task based on the following instructions: (a) “Pick and place a puck onto a shelf.” (b) “Hammer a screw on the wall.” (c) “Push the puck to a goal.”

To address this issue, we plan to investigate two strategies. First, we will introduce an explicit spatial reasoning module that models spatial relations between objects. Second, we will introduce a position-specific loss for the training objective to provide direct supervision for object localization. We expect these changes to improve alignment between the language instruction and the visual observations.

VI. PHYSICAL EXPERIMENTS

We validated AnoleVLA in physical experiments using a mobile manipulator. We evaluated whether the model can follow natural language instructions and generate trajectories in real-world settings, and reported task success rates and inference time per action chunk under limited compute and memory budgets.

A. Settings

Fig. 5 illustrates the experimental setup for the physical experiments. We replicated the standardized environment of the World Robot Summit 2020 Partner Robot Challenge/Real Space (WRS2020RS) [41], which was an international contest that focused on benchmarking daily object manipulation tasks in home environments (shown in Fig. 5(a)). Furthermore, we set an additional camera to capture a bird’s-eye view.

In the physical experiments, we used the Human Support Robot [39] developed by Toyota Motor Corporation. This

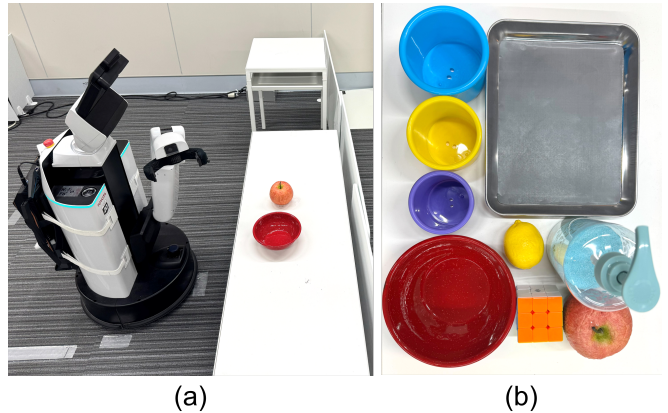


Fig. 5: (a) Robot platform and experimental environment used in the physical experiments. We used the Human Support Robot (HSR) [39] as the robot platform. (b) Everyday objects used in the experiments. We used standard YCB objects [40] for manipulation research, along with additional objects to increase diversity in appearance and size.

mobile manipulator has been used as the standard platform for the RoboCup@Home competition [42] since 2017. The robot features a total of 11 DoF, comprising 3 DoF in the mobile base, 6 DoF in the manipulator, and 2 DoF in the head. Furthermore, it is equipped with cameras mounted on both its head and end-effector. We selected the objects used in the experiments from the YCB object set [40], a standard benchmark for robot manipulation research. We also included a variety of common everyday objects (Fig. 5(b)) to improve diversity in visual appearance and physical size. In the physical experiments, we evaluated AnoleVLA across five typical manipulation tasks to demonstrate its versatility. The definitions of these tasks are as follows: ‘Move’: Move an object laterally. ‘Pick’: Grasp and lift an object. ‘Open’: Open a drawer. ‘Close’: Close a drawer. ‘Push’: Depress a bottle pump.

We used a leader-follower system [43] for data collection. A human operator manipulated a leader device to teleoperate the robot and collect trajectories. We collected 50 episodes for each task while randomly varying object placement and the robot’s initial pose, which resulted in a dataset totaling 250 episodes. We recorded each episode at a sampling rate of 10 Hz and took images from three viewpoints (external, head-mounted, and wrist-mounted cameras), along with all joint angles at each timestep. We set d_a to 11.

B. Quantitative Results

Table II shows a quantitative comparison between AnoleVLA and the baseline methods in the physical experiments. For each task, we conducted 20 trials. The resulting success rates are presented in the table. The ‘Inf. speed’ column specifies the inference speed of each method in the physical experiments.

AnoleVLA achieved an average success rate of 63%, whereas the values of VLA-Adapter, TinyVLA, and SmolVLA were 40%, 29%, and 52%, respectively. Consequently, AnoleVLA outperformed SmolVLA, the strongest among the small-scale VLAs, by 11 points for the average

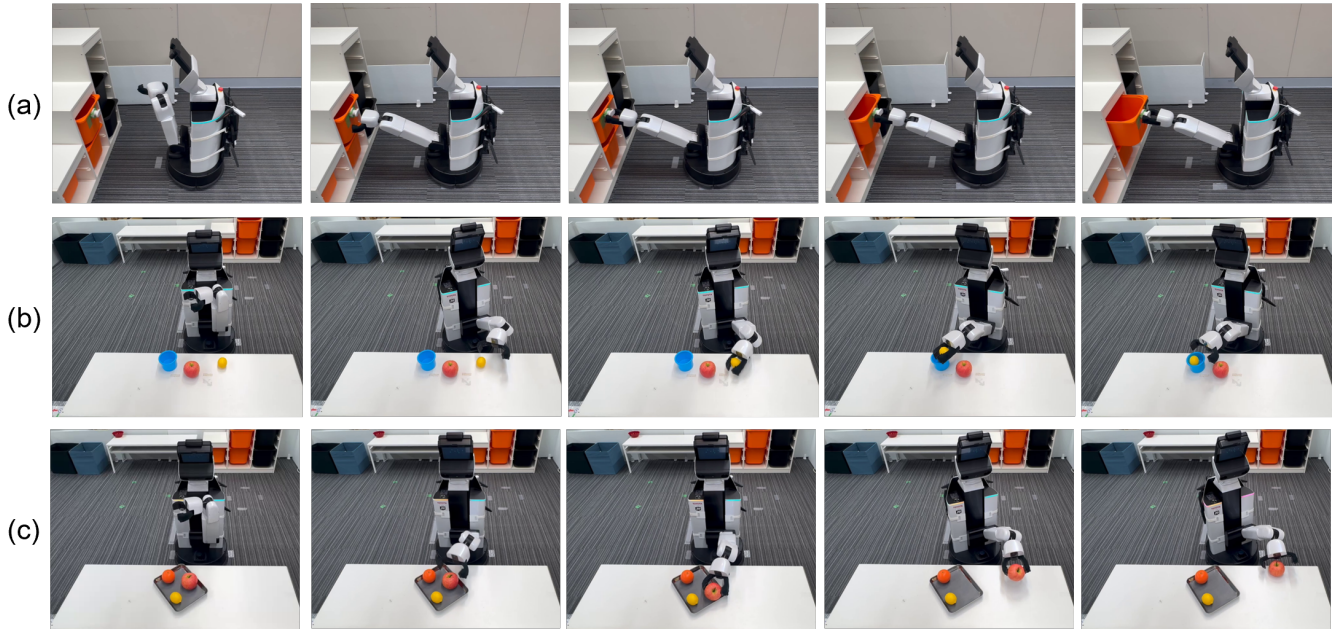


Fig. 6: Successful execution examples of AnoleVLA in the physical experiments. In each example, the robot executed the task based on the following instructions: (a) “Open the drawer.” (b) “Put the lemon into the cup.” (c) “Remove the apple from the tray.”

success rate. Furthermore, although SmoVLA performed moderately well overall, it frequently failed in spatially constrained, contact-rich tasks, achieving a success rate of only 55% on the ‘Open’ task. This drop highlights the limitation of the lack of temporal smoothness constraints for conventional VLAs, which often causes jerky movements. By contrast, AnoleVLA achieved a success rate of 75% on the ‘Open’ task. AnoleVLA leverages Mamba’s linear complexity to efficiently fuse multi-view features and uses a time-derivative loss to generate the smooth, precise trajectories essential for complex physical interactions.

Regarding inference speed, AnoleVLA achieved 216 ms/chunk. SmoVLA and $\pi_{0.5}$ took 309 and 578 ms/chunk, respectively. Therefore, AnoleVLA was approximately three times faster than $\pi_{0.5}$ while achieving the best success rate. VLA-Adapter achieved the lowest latency at 101 ms/chunk in our setup. However, it yielded substantially lower success rates, which indicates that AnoleVLA provided a better balance between the success rate and inference speed under limited compute budgets.

There are two main reasons for this significant performance gap. First, the small training dataset of only 50 episodes per task made it difficult to fine-tune $\pi_{0.5}$. Although $\pi_{0.5}$ is heavily pre-trained, massive architectures with 3B parameters generally suffer from low sample efficiency with such limited data, making effective adaptation challenging without overfitting. Second, a substantial domain gap exists regarding visual observations. The pretraining data for $\pi_{0.5}$ mainly contains table-top manipulation from fixed viewpoints; however our tasks require whole-body manipulation with continuously changing viewpoints. Consequently, the representations acquired during pre-training did not transfer effectively to our experimental setting. These findings

demonstrate that AnoleVLA is highly sample-efficient and capable of robust task acquisition even with severely limited demonstration data.

C. Qualitative Results

Fig. 6 shows three selected successful manipulation episodes with AnoleVLA in the physical experiments. Each sequence of images illustrates the $x_v^{(t)}$ in chronological order from left to right.

In episode (a), given the instruction “Open the drawer;” the robot appropriately accomplished this task by grasping the handle and pulling it forward to achieve full extension. The target task in episode (b) was specified as “Put the lemon into the cup.” The robot successfully executed the required behavior by lifting the lemon and placing it into the target container. In episode (c), the robot received the instruction sentence “Remove the apple from the tray.” It successfully executed the task by grasping the apple and relocating it to the exterior area. These examples demonstrate successful cases where AnoleVLA appropriately comprehended the desired task based on the instruction sentence, subsequently generating trajectories to complete the operation.

VII. CONCLUSIONS

In this study, we addressed the task of language-guided robotic manipulation, which involves performing object manipulation based on visual information and language instructions. The main contributions of this work are summarized as follows:

- We proposed AnoleVLA, a lightweight and high-speed VLA designed to operate efficiently even in resource-constrained environments.

- We introduced Mamba as the backbone architecture and leveraged its computationally efficient sequence processing capabilities for VLA modeling.
- We introduced a two-stage training strategy that incorporated the acceleration loss in the second phase, which complemented the velocity loss used in the initial phase.
- We evaluated AnoleVLA in both simulation and physical experiments, which demonstrated that it outperformed baseline methods in terms of success rate.

We frequently observed cases where the model failed to pinpoint the exact location of the target object, generating trajectories toward incorrect regions. To address this issue in future work, we plan to introduce mechanisms that explicitly handle spatial information or use auxiliary losses related to object localization during training.

REFERENCES

- [1] K. Black, N. Brown, J. Darpinian, K. Dhabalia, D. Driess, A. Esmail, M. R. Equi, C. Finn, N. Fusai *et al.*, “ $\pi_{0.5}$: A Vision-Language-Action Model with Open-World Generalization,” in *CoRL*, 2025.
- [2] Q. Bu, Y. Yang, J. Cai, S. Gao, G. Ren, M. Yao, P. Luo, and H. Li, “UniVLA: Learning to Act Anywhere with Task-centric Latent Actions,” in *RSS*, 2025.
- [3] M. Kim, K. Pertsch, S. Karamcheti *et al.*, “OpenVLA: An Open-Source Vision-Language-Action Model,” in *CoRL*, 2024.
- [4] A. Brohan, N. Brown, J. Carbajal, Y. Chebotar, X. Chen, K. Chormanski, T. Ding *et al.*, “RT-2: Vision-Language-Action Models Transfer Web Knowledge to Robotic Control,” in *CoRL*, 2023.
- [5] K. Black, N. Brown, D. Driess *et al.*, “ π_0 : A Vision-Language-Action Flow Model for General Robot Control,” in *RSS*, 2025.
- [6] J. Zheng, J. Li, Z. Wang, D. Liu, X. Kang, Y. Feng, Y. Zheng, J. Zou, Y. Chen *et al.*, “X-VLA: Soft-Prompted Transformer as Scalable Cross-Embodiment Vision-Language-Action Model,” in *ICLR*, 2026.
- [7] Octo Model Team, D. Ghosh, H. Walke, K. Pertsch, K. Black, O. Mees, S. Dasari, J. Hejna, C. Xu, J. Luo, T. Kreiman, Y. Tan *et al.*, “Octo: An Open-Source Generalist Robot Policy,” in *RSS*, 2024.
- [8] W. Huang, C. Wang, R. Zhang, Y. Li, J. Wu, and L. Fei-Fei, “VoxPoser: Composable 3D Value Maps for Robotic Manipulation with Language Models,” in *CoRL*, 2023, pp. 540–562.
- [9] W. Zhao, J. Chen, D. Meng, D. Mao, R. Song, and W. Zhang, “VLMPC: Vision-Language Model Predictive Control for Robotic Manipulation,” *arXiv preprint arXiv:2407.09829*, 2024.
- [10] C. Hori, M. Kambara, K. Sugiura, K. Ota, S. Khurana, S. Jain *et al.*, “Interactive Robot Action Replanning using Multimodal LLM Trained from Human Demonstration Videos,” in *ICASSP*, 2025, pp. 1–5.
- [11] Y. Ma, Z. Song, Y. Zhuang, J. Hao, and I. King, “A Survey on Vision-Language-Action Models for Embodied AI,” *arXiv preprint arXiv:2405.14093*, 2024.
- [12] K. Kawaharazuka, Y. Obinata, N. Kanazawa, K. Okada, and M. Inaba, “Robotic Applications of Pre-Trained Vision-Language Models to Various Recognition Behaviors,” in *Humanoids*, 2023, pp. 1–8.
- [13] Y. Wang, P. Ding, L. Li, C. Cui, Z. Ge, X. Tong, W. Song, H. Zhao *et al.*, “VLA-Adapter: An Effective Paradigm for Tiny-Scale Vision-Language-Action Model,” *arXiv preprint arXiv:2509.09372*, 2025.
- [14] J. Wen, Y. Zhu, J. Li, M. Zhu, Z. Tang, K. Wu, Z. Xu, N. Liu *et al.*, “TinyVLA: Towards Fast, Data-Efficient Vision-Language-Action Models for Robotic Manipulation,” *IEEE RA-L*, 2025.
- [15] M. Shukor, D. Aubakirova, F. Capuano, P. Kooijmans, S. Palma *et al.*, “SmolVLA: A Vision-Language-Action Model for Affordable and Efficient Robotics,” *arXiv preprint arXiv:2506.01844*, 2025.
- [16] A. O’Neill, A. Rehman *et al.*, “Open X-Embodiment: Robotic Learning Datasets and RT-X Models: Open X-Embodiment Collaboration,” in *ICRA*, 2024, pp. 6892–6903.
- [17] A. Brohan, N. Brown, J. Carbajal, Y. Chebotar *et al.*, “RT-1: Robotics Transformer for Real-World Control at Scale,” in *RSS*, 2023.
- [18] H. Walke, K. Black, A. Lee, M. J. Kim, M. Du, C. Zheng, T. Zhao *et al.*, “BridgeData V2: A Dataset for Robot Learning at Scale,” in *CoRL*, 2023.
- [19] D. Qu, H. Song, Q. Chen, Y. Yao, X. Ye, Y. Ding, Z. Wang, J. Gu, B. Zhao, D. Wang *et al.*, “SpatialVLA: Exploring Spatial Representations for Visual-Language-Action Model,” *RSS*, 2025.
- [20] Q. Zhao, Y. Lu, M. Kim, Z. Fu, Z. Zhang, Y. Wu, Z. Li, Q. Ma, S. Han, C. Finn *et al.*, “CoT-VLA: Visual Chain-of-Thought Reasoning for Vision-Language-Action Models,” in *CVPR*, 2025, pp. 1702–1713.
- [21] R. Zheng, Y. Liang, S. Huang, J. Gao, H. Daumé, A. Kolobov *et al.*, “TraceVLA: Visual Trace Prompting Enhances Spatial-Temporal Awareness for Generalist Robotic Policies,” in *ICLR*, 2025.
- [22] T. Yu, D. Quillen, Z. He, R. Julian, K. Hausman, C. Finn, and S. Levine, “Meta-World: A Benchmark and Evaluation for Multi-Task and Meta Reinforcement Learning,” in *CoRL*, 2019.
- [23] A. Gu, K. Goel, and C. Ré, “Efficiently Modeling Long Sequences with Structured State Spaces,” in *ICLR*, 2022.
- [24] A. Gu, K. Goel, A. Gupta, and C. Ré, “On the Parameterization and Initialization of Diagonal State Space Models,” in *NeurIPS*, vol. 35, 2022, pp. 35971–35983.
- [25] A. Gu and T. Dao, “Mamba: Linear-Time Sequence Modeling with Selective State Spaces,” in *CoLM*, 2024.
- [26] H. Zhao, M. Zhang, W. Zhao, P. Ding, S. Huang, and D. Wang, “Cobra: Extending Mamba to Multi-Modal Large Language Model for Efficient Inference,” in *AAAI*, 2025.
- [27] Y. Qiao, Z. Yu, L. Guo, S. Chen, Z. Zhao, M. Sun, Q. Wu, and J. Liu, “VLMamba: Visual State Space Model for View-Language Reasoning,” *arXiv preprint arXiv:2403.13595*, 2024.
- [28] X. He, L. Wei, J. Ouyang, M. Liao, L. Xie, and Q. Tian, “EMMA: Efficient Multimodal Understanding, Generation, and Editing with A Unified Architecture,” *arXiv preprint arXiv:2512.04810*, 2025.
- [29] J. Liu, M. Liu, Z. Wang, P. An, X. Li, K. Zhou, S. Yang, R. Zhang, Y. Guo *et al.*, “RoboMamba: Efficient Vision-Language-Action Model for Robotic Reasoning and Manipulation,” in *NeurIPS*, 2024.
- [30] S. Wang, L. Wang, S. Zhou, J. Tian, J. Li, H. Sun *et al.*, “FlowRAM: Grounding Flow Matching Policy with Region-Aware Mamba Framework for Robotic Manipulation,” in *CVPR*, 2025, pp. 12176–12186.
- [31] I. Nematollahi, B. DeMoss, A. Chandra, N. Hawes, W. Burgard, and I. Posner, “LUMOS: Language-Conditioned Imitation Learning with World Models,” in *ICRA*, 2025, pp. 8219–8225.
- [32] Y. Yoo, J. Hu, Y. Zhu, B. Liu, Q. Liu, R. Martín-Martín, and P. Stone, “RoboSSM: Scalable In-context Imitation Learning via State-Space Models,” in *CoRL*, 2025, pp. 1–8.
- [33] X. Jia, Q. Wang, A. Donat, B. Xing, G. Li, H. Zhou, O. Celik, D. Blessing *et al.*, “Mall: Improving Imitation Learning with Selective State Space Models,” in *CoRL*, 2025, pp. 3888–3907.
- [34] J. Cao, Q. Zhang, J. Sun, J. Wang, H. Cheng, Y. Li, J. Ma *et al.*, “Mamba Policy: Towards Efficient 3D Diffusion Policy with Hybrid Selective State Models,” in *IROS*, 2025, pp. 11359–11366.
- [35] N. Oh, J. Jang, M. Jung, and D. Park, “DiSPo: Diffusion-SSM based Policy Learning for Coarse-to-Fine Action Discretization,” *arXiv preprint arXiv:2409.14719*, 2024.
- [36] T. Tsuji, “Mamba as a Motion Encoder for Robotic Imitation Learning,” *IEEE Access*, vol. 13, pp. 69941–69949, 2025.
- [37] M. Tschannen, A. Gritsenko *et al.*, “SigLIP 2: Multilingual Vision-Language Encoders with Improved Semantic Understanding, Localization, and Dense Features,” *arXiv preprint arXiv:2502.14786*, 2025.
- [38] M. J. Kim, C. Finn, and P. Liang, “Fine-Tuning Vision-Language-Action Models: Optimizing Speed and Success,” *arXiv preprint arXiv:2502.19645*, 2025.
- [39] T. Yamamoto, K. Terada, A. Ochiai, F. Saito *et al.*, “Development of Human Support Robot as the research platform of a domestic mobile manipulator,” *ROBOMECH Journal*, vol. 6, no. 1, p. 4, 2019.
- [40] B. Calli, A. Walsman, A. Singh, S. Srinivasa *et al.*, “Benchmarking in Manipulation Research: Using the Yale-CMU-Berkeley Object and Model Set,” *IEEE RAM*, vol. 22, no. 3, pp. 36–52, 2015.
- [41] “World Robot Summit 2020 Partner Robot Challenge Real Space Rules & Regulations,” 2020. [Online]. Available: https://wrs.nedo.go.jp/wrs2020/challenge/download/Rules/DetailedRules_Partner_EN.pdf
- [42] L. Iocchi, D. Holz, J. Solar, K. Sugiura, and T. Zant, “RoboCup@Home: Analysis and results of evolving competitions for domestic and service robots,” *AIJ*, vol. 229, pp. 258–281, 2015.
- [43] R. Takanami, P. Khrapchenkov, S. Morikuni, J. Arima, Y. Takaba *et al.*, “Airoa moma dataset: A large-scale hierarchical dataset for mobile manipulation,” *arXiv preprint arXiv:2509.25032*, 2025.